AGU PUBLICATIONS

Water Resources Research

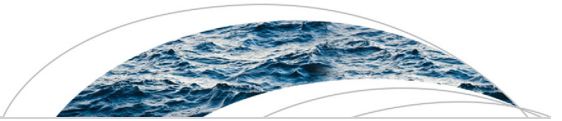

RESEARCH ARTICLE
10.1002/2014WR016035

Key Points:
- Basin hydrologic response is a function of soil moisture distributional features
- An information-based dimensionless index of hydrologic complexity is applied
- The complexity index characterizes soil moisture distributional features

Correspondence to:
A. Castillo,
aldrichcastillo@gmail.com

Citation:
Castillo, A., F. Castelli, and D. Entekhabi (2015), An entropy-based measure of hydrologic complexity and its applications, *Water Resour. Res.*, *51*, 5145–5160, doi:10.1002/2014WR016035.

Received 11 JUL 2014
Accepted 10 MAY 2015
Accepted article online 15 MAY 2015
Published online 14 JUL 2015

An entropy-based measure of hydrologic complexity and its applications

Aldrich Castillo[1,2], Fabio Castelli[3], and Dara Entekhabi[1,2]

[1]Department of Civil and Environmental Engineering, MIT, Cambridge, Massachusetts, USA, [2]Center for Environmental Sensing and Modeling, Singapore-MIT Alliance for Research and Technology, Singapore, [3]Department of Civil and Environmental Engineering, University of Florence, Florence, Italy

Abstract Basin response and hydrologic fluxes are functions of hydrologic states, most notably of soil moisture. However, characterization of hillslope-scale soil moisture is challenging since it is both spatially heterogeneous and dynamic. This paper introduces an entropy-based and discretization-invariant dimensionless index of hydrologic complexity $\mathcal{H}$ that measures the distance of a given distribution of soil moisture from a Dirac delta (most organization) and a uniform distribution (widest distribution). Applying the distributed hydrologic model MOBIDIC to seven test basins with areas ranging 10^0-10^3 km^2 and representing semiarid and temperate climates, $\mathcal{H}$ is shown to capture distributional characteristics of soil moisture fields. It can also track the temporal evolution of the distributional features. Furthermore, this paper explores how basin attributes affect the characteristic $\mathcal{H}$, and how $\mathcal{H}$ can be used to explain interbasin variability in hydrologic response. Relationships are found only by grouping basins with the same climate or size. For the semiarid basins, $\mathcal{H}$ scales with catchment area, topographic wetness, infiltration ratio, and base flow index; while $\mathcal{H}$ is inversely related to relief ratio.

1. Introduction

1.1. Overview

The hydrologic response (HR) of a basin pertains to how precipitation is partitioned into streamflow, evapotranspiration (ET), and change in storage. These fluxes can be further partitioned, e.g., streamflow into quick flow and base flow. The ability to explain or predict the response or the spatiotemporal variability of the above mentioned hydrologic fluxes and states has many important applications such as flood forecasting, water budget studies, and design of efficient hydrologic observing systems. However, it is difficult to explain much less predict the response because it is the combined manifestation of many complex and interrelated factors that naturally vary both in space and time, and act over a variety of scales.

Most studies of hydrologic response focus only on the streamflow component of the hydrologic response and how it is influenced by a single factor or class of factors such as runoff contributing areas and routing processes, catchment shape, topographic convergence index [*Beven and Kirby*, 1997], geomorphology [*Rodriguez-Iturbe and Rinaldo*, 1997; *Di Lazzaro*, 2008], and storm characteristics [*Vivoni et al.*, 2007]. Several studies with a broader focus investigate the hydrologic response across several basins. Some of these studies are summarized and compared in Table 1. The majority used stream gauge measurements while *Berger and Entekhabi* [2001] used numerically simulated streamflow, and [*Cerdan et al.*, 2004; *Buttle et al.*, 2004] used both observed and simulated streamflow. These selected studies also show how over the years the approach generally progressed in terms of the number and coverage of basins used, the number and types of predictors and measures of response considered, and the complexity of numerical models employed. Unfortunately, the findings of these studies are not general but rather specific to the region or season studied, or the scale considered. For instance, based on different studies and in no particular order, the interbasin variability of runoff ratio (streamflow Q divided by precipitation P) is found to be controlled mainly by physiography [*Zecharias and Brutsaert*, 1988; *Sefton and Howarth*, 1998], climate [*Merz et al.*, 2006; *van Dijk*, 2010], land use [*Cerdan et al.*, 2004], preferential flow paths and soil depth [*Buttle et al.*, 2004]; or a combination of these attributes [*Berger and Entekhabi*, 2001; *Sankarasubramanian and Vogel*, 2002].

Table 1. Comparison of Select Previous Studies That Investigate the Use of Multiple Predictors of Hydrologic Response Through Hydrograph Analysis

Reference	*Zecharias and Brutsaert* [1988]	*Sefton and Howarth* [1988]	*Berger and Entekhabi* [2001]	*Sankarasubramanian and Vogel* [2002]
# of basins	19	60	10	1305
Area	8–180 km^2	9–900 km^2	10–325 km^2	>50 km^2
Location	Appalachians, US	England and Wales	Continental US	Continental US
Predictors of HR	8 Topography and geomorphology	29 Physiography, climate and land cover	8 Physiography and climate	4 Physiography and climate
Measures of HR	Base flow Q_{bf}	Streamflow Q	Q/P, ET/E_p, θ, riparian zones extent	Runoff ratio Q/P
Streamflow data	Observed	Observed	Modeled	Observed
Hydrologic model	None	Lumped and semiphysics-based	Semidistributed equilibrium model	None
Findings	98% of Q_{bf} variance $f(A$, relief, length of perennial streams)	63% of Q variance $=f$(elevation, TWI, stream freq., A)	87% of Q/P variance $= f(P/E_p$, slope, stream density, infil. cap.)	71% of Q/P variance $= f(P/E_p$, slope, stream density, infil. cap.)
Reference	*Cerdan et al.*, [2004]	*Buttle et al.* [2004]	*Merz et al.* [2006]	*van Dijk* [2010]
# of basins	3 + 40	1	337	183
Area	Plot–10 km^2	3.2 ha	80–10,000 km^2	51–1780 km^2
Location	France	Canadian Shield	Austria	Australia
Predictors of HR	Physiography, land use	Topography, soils, and plants	Physiography, climate and land cover/use	Physiography, climate and land cover
Measures of HR	Streamflow Q	$Q/P, Q, Q_{bf}$, GW depth	Streamflow Q	Q, Q_{bf}
Streamflow data	Observed and modeled	Observed and modeled	Observed	Observed
Hydrologic model	Distributed conceptual model	Semidistributed physics-based model	None	Simple linear-reservoir
Findings	R/P decreases as A and % of arable land increase	Dominant controls are preferential flow paths and soil depth	Q/P is controlled by mean P and little by soil type or land cover	Q and Q_{bf} are controlled by E_p and monthly P

The basin attributes (e.g., climate, topography, soil texture, etc.) are indirectly controlling hydrologic response. There is also strong and long-standing evidence that vegetation distribution is a key determinant and determines the hydrologic response of catchment, especially in water-limited evaporation regimes [*Mendez-Barroso and Vivoni*, 2010; *Mendez-Barroso et al*., 2014]. These and other attributes affect hydrologic response principally through the soil moisture state variable of catchment hydrology. Basin response and hydrologic fluxes are direct functions of distributed hydrologic states, most notably of soil moisture, θ, which controls the partitioning of rainfall into infiltration and runoff, and also controls land surface temperature through its effect on the partitioning of available energy into sensible and latent heat fluxes. The distributional features of θ, both at the surface and in the root-zone, are important determinants of the partitioning of atmospheric precipitation and radiative forcing into hydrologic and heat fluxes across the basin [*Grayson et al*., 1997; *Penna et al*., 2009; *Diek et al*., 2014]. The characterization of θ distributional features is itself challenging since θ is both heterogeneous and dynamic. Moreover, θ is dynamic due to the intermittency, seasonality, and interannual variability of meteorological forcings.

As important and as direct an influence on hydrologic response as they may be, the spatial and temporal distributional features of θ at catchment scale have not been routinely observed. Only recently has the scientific community dedicated significant efforts to addressing this problem through pervasive ground-based monitoring networks [*Dorigo et al*., 2011], remote sensing [*Moghaddam et al*., 2013], etc. Meanwhile, in attempts to capture some of the most salient features of the distribution, there is a rich set of early studies that work with the mean (central tendency) and the dispersion (variance) of θ distribution across basins. Since θ is a bounded random variable, the spatial variance $\sigma^2(\theta)$ usually increases as the basin mean soil moisture $\bar{\theta}$ distances from the dry or wet extrema. In semiarid regions, $\sigma^2(\theta)$ generally increases with $\bar{\theta}$ [*Fernandez and Ceballos*, 2003]. In humid regions, $\sigma^2(\theta)$ generally decreases as $\bar{\theta}$ increases [*Meyles et al*., 2003; *Teuling and Troch*, 2005]. And in temperate regions, $\sigma^2(\theta)$ peaks at intermediate $\bar{\theta}$ [*Famiglietti et al*., 1999, 2008; *Lawrence and Hornberger*, 2007]. *Mahmood and Vivoni* [2008, 2011] show that both the spatial autocorrelation length and spatial coefficient of variation (CV) not only characterize the spatial soil moisture distribution but also partially control its temporal evolution.

In a closely related study to the one reported here but with different focus and approach, *Nippgen et al*. [2011] link mean time-to-response of basin discharge to landscape structure and climate. They focus on a

basin in Montana with seven instrumented subcatchments. The region has significant snow hydrology and vegetation gradient with elevation. They fit a convolution linear transfer model (taken to be the gamma function) that translates a measured effective daily rainfall and snowmelt into daily output (daily discharge). The *Nippgen et al*. [2011] landscape features are overlapping with the metrics used in this study and particularly well suited for their experimental basin. They include mean and median landscape slope, distance to creek, gradient to creek, hillslope power, terrain convergence, upslope accumulated area, ratio of riparian area to hillslope area, average tree height, potential annual solar insolation, and presence of geologic strata. They find that the mean (time) hydrologic response of the catchments has no significant correlations with landscape variables and modeled mean catchment response with the exception of mean convergence terrain convergence which shows a very strong statistical correspondence. More importantly they find that the effect of one or two variables superimposed onto the others can explain more of the variabilities. Section 4 in *Nippgen et al*. [2011] poses a number of important questions and hypotheses and their Figure 8 and Table 5 contain the results relevant to this study. Whereas *Nippgen et al*. [2011] focus on time scale of catchment response to excess precipitation, in this study we focus on hydrologic response in terms of precipitation partitioning and marginal distribution of surface soil moisture in the catchment.

In this paper, we also focus on the spatial distribution of soil moisture across the basin as the intermediary between basin attributes (e.g., climate, topography, etc.) and hydrologic response (e.g., partitioning of precipitation into runoff, evaporation, etc.). We introduce a statistical measure of the distribution which is more informative than mean and variance alone. For illustration, the measure is evaluated over time using numerically simulated soil moisture fields for different seasons and climate conditions. Furthermore, the measure is evaluated for water held in storage under distinct physical conditions. Soil water is partitioned into moisture that can readily drain under gravity (gravitational water) and water that is held in storage under capillary action (capillary water). Water from each of these reservoirs is accessible to different hydrologic fluxes. Gravitational water mostly contributes to quick runoff and groundwater recharge. Capillary water mostly contributes to evaporation.

The measure applied to the marginal probability density distributions of soil moisture is based on information theory. The measure is termed hydrologic complexity since it is designed to characterize the complexity of the hydrologic response of basins. This assumes that the soil layer has first-order control on the hydrologic response of basins, while deeper hydrogeology only has indirect influence through the bidirectional soil moisture—groundwater interactions such as percolation, return flow (wetting from below), and capillary rise. Other complications such as karst geology and deep subsurface runoff along soil-bedrock interface, that strongly influence the hydrologic response of some basins, are not considered by the proposed measure of hydrologic complexity.

In general, the least hydrologically complex basin is one that can be characterized by the so-called bucket representation. For example, the runoff response is precipitation exceedance of a soil moisture deficit value. For this least complex basin, the soil moisture distribution across the basin (marginal probability density function) is a Dirac delta function. The hydrologic complexity metric $\mathcal{H}$ for this basin, as introduced in this study, is zero. In the most complex basin, the hydrologic response is considered complex because storms of all sizes lead to some hydrologic response like runoff. Also the other hydrologic fluxes like base flow and evaporation are working to balance the basin water budget at all times. The marginal probability density function of such a basin is wide and variable across the possible values for the hydrologic state. In the limit, the distribution of the bounded soil moisture random variable for most complex basins is uniform across the soil moisture range. $\mathcal{H}$ approaches unity under these conditions.

The hydrologic complexity $\mathcal{H}$ is evaluated for several basins with different topographic conditions, drainage areas, and climates. We examine basin attributes (topography, slope, climate, etc.) that influence the distribution of soil moisture in order to determine which attributes affect the hydrologic complexity and hence the distributional features of soil moisture across the basin most. We also explore whether the basin characteristic hydrologic complexity $\mathcal{H}$ is related to some traditional measures of basin hydrologic response.

2. Entropy as an Organizing Principle

Entropy is a measure of the disorder or uncertainty of a system. Usually entropy is expressed in terms of the discrete or Shannon entropy H which is defined for a discrete random variable X with potential states $\{x_1, x_2, \ldots, x_N\}$ and probability mass function (PMF), $p(x)$, as:

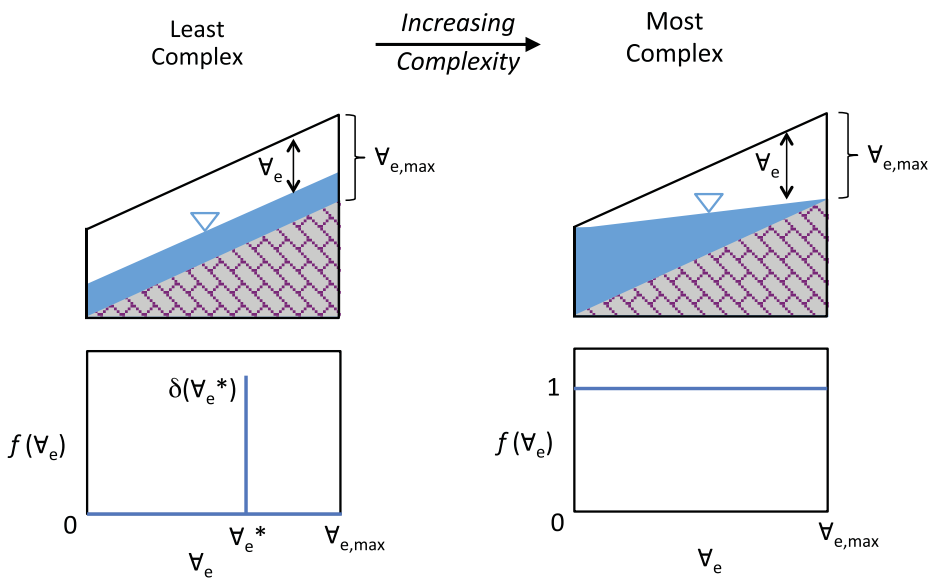

Figure 1. Conceptual diagram of the limiting cases: the soil water deficit is (left) the same across the basin; and (right) uniformly distributed from zero to a maximum value. Bottom plots show the probability density functions of $\forall_e$.

$$H(X) = -\sum_{i=1}^{N} p(x_i) \log p(x_i) \tag{1}$$

Singh [2011] provides a review of the use of entropy theory in hydrology, and suggests its use as an organizing principle in hydrology.

As discussed, basin response and hydrologic fluxes are functions of states most notably of soil moisture which is usually expressed as either volumetric soil moisture θ [L^3/L^3], or percent saturation. It can also be expressed as available storage $\forall_e$ [L] which is particularly useful in water balance analysis. Interchangeably, $\forall_e$ can be referred to as the soil water deficit. When the soil is saturated, $\forall_e = 0$, whereas when the soil is dry, $\forall_e = \forall_{e,max}$ which is simply the product of effective porosity and soil depth.

Figure 1 shows the conceptual diagram of the two end-members of the possible spatial distributions of $\forall_e$ in a basin. The simplest case is when $\forall_e$ is the same across the basin. The probability density function (PDF), $f(\forall_e)$, is a Dirac delta function as shown in the bottom plot. For this case, the basin can be represented by a single bucket with deterministic response or spatially constant fluxes. The most complex case is when $f(\forall_e)$ is equally likely to take any value within its range, i.e., it is uniformly distributed from 0 to $\forall_{e,max}$. For this case, the fluxes are spatially variable and the response is complicated. Naturally of course, a basin or a hillslope will have a spatial distribution of $\forall_e$ that is intermediate between these limiting cases. It is useful then to have a metric to quantify the distance of a given distribution of $\forall_e$ from these limiting distributions.

With this motivation, *Martina and Entekhabi* [2006] introduced a dimensionless index of hydrologic complexity they defined as the Shannon entropy of $\forall_e$, normalized by log(N), where N is the number of bins used to generate the PMF. The normalization constrains the values of the index between zero and unity. In this paper, we present a revised formulation of this index that makes its value invariant also to discretization.

Let X be the relative soil water deficit, with spatial distribution $f(x)$ for $x \in [0, 1]$, and $\int_0^1 f(x)dx = 1$:

$$X = \forall_e / \forall_{e,max} \tag{2}$$

The revised dimensionless measure of hydrologic complexity $\mathcal{H}$ is defined as,

$$\mathcal{H} = \exp[h(X)] \tag{3}$$

where $h(X)$ is the differential entropy of X,

$$h(X) = -\int f(x) \log f(x)\, dx \tag{4}$$

With the given definition of X, $h(X)$ above is also equal to the negative of the relative entropy, otherwise known as the Kullback-Liebler divergence D_{KL}, of $f(x)$ from a reference distribution $g(x)$ which in this case is a uniform distribution in the interval $[0, 1]$.

$$h(X) = -D_{KL}(f||g) \quad \text{for } x \in [0, 1], \text{ with arbitrary } f(x), \text{ and } g(x) \sim \mathrm{U}[0, 1] \tag{5}$$

An important property of D_{KL} is that it is always nonnegative with $D_{KL} = 0$ if and only if $f(x)$ and $g(x)$ have the same support set and $f(x) = g(x)$ everywhere in the support set [*Michalowicz et al.*, 2014].

The complete derivation of $\mathcal{H}$ can be found in *Castillo* [2014]. In this paper, we would like to point out that $\mathcal{H}$ is (i) computed based on differential entropy instead of Shannon entropy; (ii) computed for random variables X with values strictly in the interval 0–1; (iii) uses the Kullback-Leibler divergence to ensure that $h(X) \leq 0$; and (iv) applies an exponential transformation so that $\mathcal{H} \in [0, 1]$, with $\mathcal{H} = 0$ for the simplest, and $\mathcal{H} = 1$ for the most complex case, respectively.

Figure 2 (top-left and bottom-left plots) corresponds to the two limiting cases shown in Figure 1. The $\mathcal{H}$ for these two cases are 1 and 0 reflecting the most complex $(\mathcal{H} = 1)$ and the most organized $(\mathcal{H} = 0)$. For two intermediate complexity cases (right plots), the $\mathcal{H}$ takes on values in between 0 and 1. Figure 2 shows the invariance of the measure $\mathcal{H}$ to discretization N or Δx with $\Delta x = 1/N$.

$\mathcal{H}$ can be used to (i) analyze how the complexity of the spatial distribution of X evolves over time; and (ii) compare the characteristic distribution of X for different basins. The remainder of this paper demonstrates the latter application. The hydrology of multiple test basins with areas ranging $10^0 - 10^3$ km^2 and representing semiarid and temperate climates is simulated using a distributed hydrologic model. Next we investigate (i) how the distributional features of soil water deficit evolve over time; (ii) what factors (physiography, spatial scale, climate, etc.) affect the characteristic $\mathcal{H}$; and (iii) how the characteristic $\mathcal{H}$ is related to other traditional measures of basin hydrologic response.

3. Methods

3.1. Test Basins

Table 2 identifies the seven test basins. The test basins are chosen to represent two contrasting climatic regimes—temperate and semiarid, and represent four orders of catchment area. In addition, the test basins cover test sites of NASA's AirMOSS (airmoss.jpl.nasa.gov) and SoilSCAPE (soilscape.usc.edu) projects. The goals of both projects include the investigation of the space-time variability of soil moisture and the design of effective and efficient in situ and airborne observing systems to support spaceborne platforms for measuring soil moisture. Soil moisture observations from these projects were used for model calibration. The first column lists the basin ID with the letter denoting the climate ("S" for semiarid and "T" for temperate) and the number denoting the size of the basin ("0," "1," "2," and "3," for areas of about 10^0, 10^1, 10^2, and 10^3 sq km, respectively). The last column shows the dominant land cover and land use. The location maps of these basins are shown in Figure 3. Basins S0, S1, S2, S3, and T0 cover field sites of the Soil moisture Sensing Controller and oPtimal Estimator (SoilSCAPE) Project, see *Moghaddam et al.* [2013]. T2 and T3 are tests basins in the Distributed Model Intercomparison Project (DMIP), see *Reed et al.* [2004]. Note that basin S3 includes some upland areas with snowmelt, however this process was not considered in the study. Additional properties of the test basins are listed in Table 3.

In this exploratory study, we focus on two climates and basins that span four orders of magnitude in area. One climate regime has strong seasonality and one is without a distinct precipitation season. We emphasize that more basins should be tested beyond the limited set used in this study in order to (i) further test the applicability of $\mathcal{H}$ under different conditions; and (ii) establish more robust relationships between $\mathcal{H}$ and catchment attributes influencing hydrologic response.

3.2. The Hydrologic Model MOBIDIC

Numerical simulations of the test basins are performed using the Modello Bilancio Idrologico DIstributo e Continuo (MOBIDIC), a raster-distributed and continuous catchment hydrologic model that solves mass and

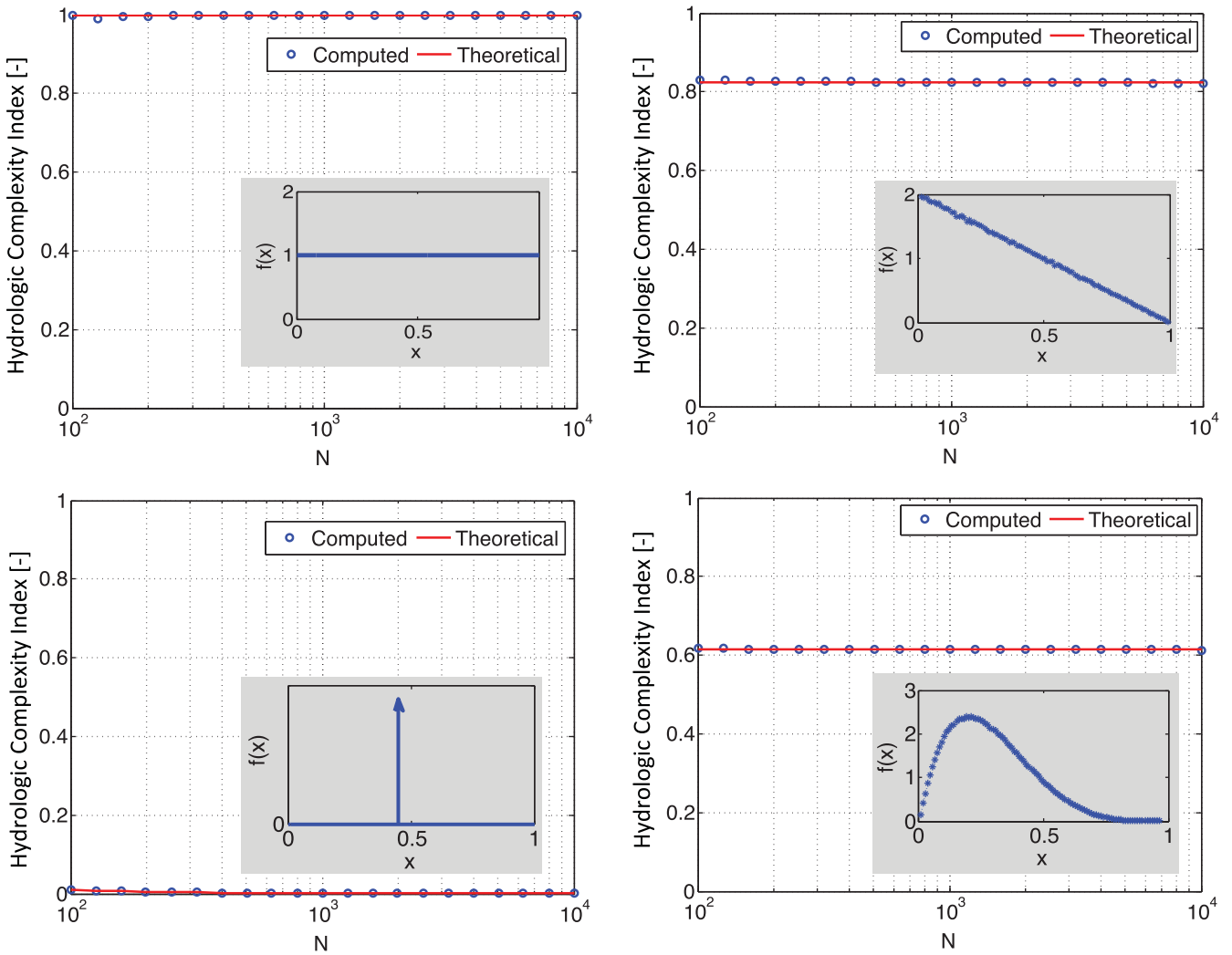

Figure 2. The revised dimensionless hydrologic complexity index $\mathcal{H}$ is independent of numerical discretization (N= number of bins). The insets show the PDFs used.

energy balance simultaneously. MOBIDIC represents the basin by simulating a system of water reservoirs and the mass and energy fluxes between them. For computational parsimony and to account for the different roles of gravity and capillary forces in storing and moving soil water, each plan element (i.e., pixel) of soil is represented by a single soil layer divided into a gravity reservoir composed of large pores which drain under gravity, and a capillary reservoir composed of small pores that do not drain under gravity and hold water under capillary action. The volume capacity per unit area [L^3/L^2] of these reservoirs is denoted by $W_{g,max}$, and $W_{c,max}$, respectively, which are parameterized as,

$$W_{g,max} = d\,(\theta_{sat} - \theta_{fld}) \tag{6}$$

$$W_{c,max} = d\,\theta_{fld} \tag{7}$$

where d [L] is the depth of the modeled soil; and θ_{sat} and θ_{fld} [L^3/L^3] are the volumetric soil moisture at saturation and field capacity, respectively. θ_{sat} and θ_{fld} are initialized based on soil texture type and using the range of values reported by *Rawls et al.* [1982].

Within each computational time step, dt [T], the hydrologic fluxes [$L\,T^{-1}$] linking elements across the landscape include precipitation P, infiltration-excess runoff R_H, partial-area (saturation from below) runoff R_D, return flow R_R, total runoff R_T, infiltration I, absorption Q_{as} from W_g to W_c, percolation Q_{per}, lateral subsurface

Table 2. Description of the Test Basins

ID	Name and Location	Climate	Land Cover/Use
S0	Tonzi Ranch, CA	Semiarid	Woody savanna
S1	Vaira Ranch, CA	Semiarid	Grassland, woody savanna, shrubland
S2	Willow Creek Basin, CA	Semiarid	Woody savanna, grassland, shrubland
S3	San Joaquin R.B., CA	Semiarid	Grassland, farmland, woody savanna
T0	SOILSCAPE site, Canton, OK	Temperate	Pasture with some trees
T2	Baron Fork R.B., Dutchmills, AR	Temperate	Pasture, forest
T3	Blue River Basin, OK	Temperate	Grassland, farmland, woodlands

flow Q_L, capillary rise Q_{cap}, and evapotranspiration E. These water fluxes can be limited by the available water to be transported, the available receiving storage, or the allowable transport rate.

The water content states of the soil gravity and capillary reservoirs evolve according to equations (8) and (9). The gravity storage is filled by infiltration and lateral subsurface flow from upstream cell(s). It is depleted by absorption into available capillary storage, percolation to deeper soil, and lateral subsurface flow to downstream cell. The subscripts "up" and "down" denote incoming flow from upstream cell(s), and outgoing flow to downstream cell, respectively, which are determined using D8 flow routing [*Tarboton*, 1997]. If $W_g > W_{g,max}$ (caused by high $Q_{L,up}$), then the excess gravity water will be released to the surface as return flow. Meanwhile, in addition to absorption from gravity storage, the available capillary storage is also filled by capillary rise from deeper soil or from groundwater. The capillary storage is only depleted by evapotranspiration.

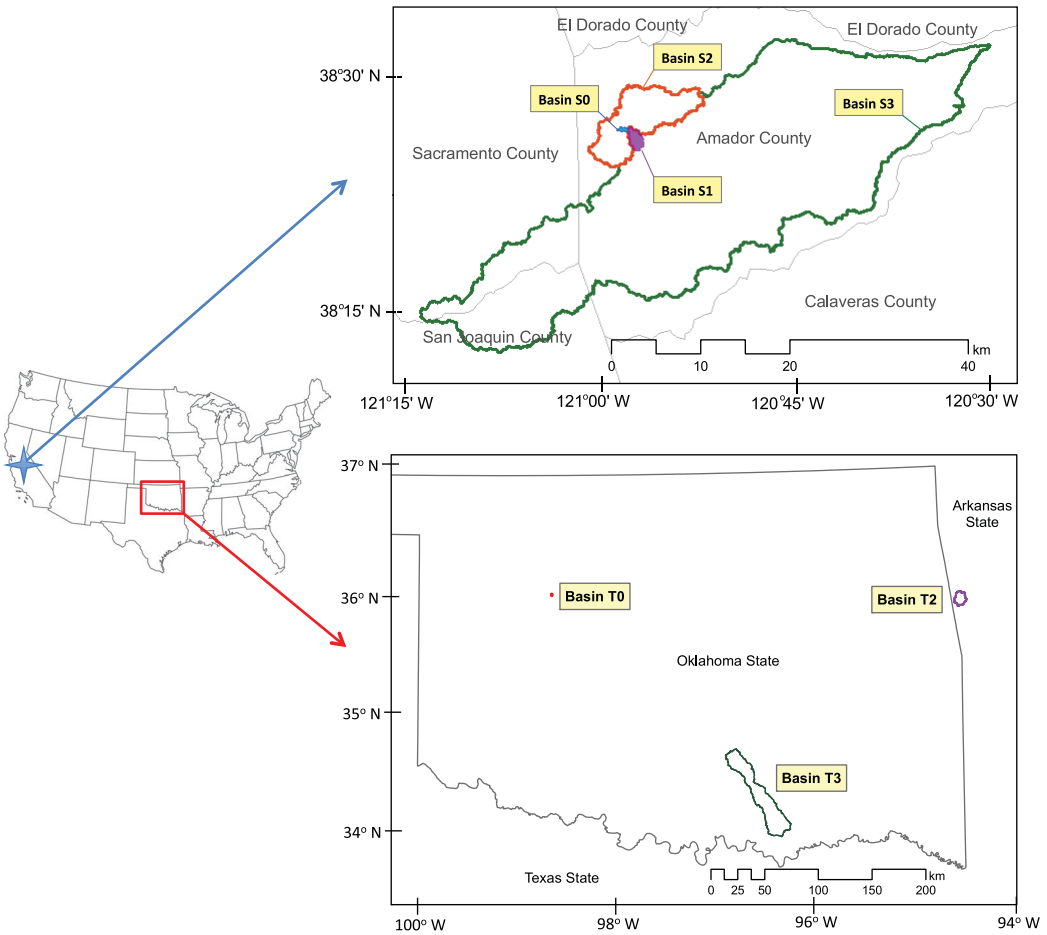

Figure 3. Location of the test basins: (top) nested semiarid basins in California; and (bottom) temperate basins in Oklahoma-Arkansas.

Table 3. Properties of the Test Basins

		Topography		Geomorphology		Soil Properties				Climate		Storm Properties		Mixed
ID	Area (km^2)	Relief (m)	s_{50}	D_d (km^{-1})	L (km)	$\overline{K_s}$(mm/h)	$\bar{d}$ (mm)	$\overline{\theta_{fld}}$	$\overline{\theta_{sat}}$	$\bar{P}$ (mm/yr)	$\overline{E_p}/\bar{P}$	i_s (mm)	t_s (h)	I_r
S0	0.45	34	0.04	2.67	0.98	28	368	0.15	0.24	569	3.71	11.1	14.4	0.028
S1	3.09	76	0.14	2.42	2.92	45	353	0.18	0.30	579	3.73	11.1	14.4	0.017
S2	54	316	0.08	2.17	19.2	17	842	0.24	0.43	576	3.50	11.1	14.4	0.045
S3	852	1278	0.18	1.20	91.2	6	613	0.14	0.31	580	3.48	11.1	14.4	0.014
T0	0.45	18	0.03	0.73	0.16	38	1113	0.15	0.29	1210	1.62	14.4	9.8	0.039
T2	108	252	0.11	1.95	18.9	11	594	0.16	0.30	1027	1.69	9.0	12.5	0.066
T3	1259	242	0.03	0.36	143.	7	1483	0.15	0.41	941	1.92	10.1	13.9	0.104

$$dW_g / dt = I + Q_{L,up} - Q_{as} - Q_{per} - Q_{L,down} - R_R \tag{8}$$

$$dW_c / dt = Q_{as} + Q_{cap} - E \tag{9}$$

Infiltration rate can be limited by soil hydraulic conductivity K_s, while adsorption, percolation, and lateral subsurface flow, are computed using equations (10)–(12), respectively. κ, γ, and β are dimensionless parameters with values from 0 to 1.

$$Q_L = \beta W_g \tag{10}$$

$$Q_{as} = \kappa (W_{g,max} - W_g) \tag{11}$$

$$Q_{per} = \gamma W_g \tag{12}$$

For a more detailed discussion of the mass and energy balance of MOBIDIC along with the formulation of each of the mass and energy fluxes, the reader is referred to *Castelli et al.* [2009] and *Castillo et al.* [2014].

MOBIDIC is currently being used in the system of flood forecasting [*Castelli et al.*, 2006] and sustainable water management [*Castelli et al.*, 2009] of the Arno River Basin Authority in Italy. In our recent paper [*Castillo et al.*, 2014], using two test sites with different climates (semiarid and subhumid) and groundwater connectivity, we showed that MOBIDIC can capture the magnitude range and dynamics of observed depth-averaged soil moisture as accurately as a benchmark model that uses multiple soil layers and employs the nonlinear Richards Equation to model flow in unsaturated soils.

Development of a MOBIDIC model for a certain basin includes preprocessing of topographic and geomorphologic model inputs, such as pit-filling of the DEM, determination of flow directions, computation of contributing area, and delineation of the river network and the basin boundary. Other required model inputs are land cover and soil maps, which are in turn used to derive parameters such as albedo and K_s. MOBIDIC can output time series of streamflow Q and base flow Q_{bf} at any point along the river network, and hydrologic fluxes (e.g., I, R_T, and E) and states (e.g., W_c and W_g) across the basin.

In the current study, the MOBIDIC models for test basins S2, S3, T2, and T3, were calibrated mainly against observed streamflow, whereas test basins S0, S1, and T0, where streamflow observations are not available, were calibrated mainly against observed soil moisture fields. In addition, for all the test basins, a number of qualitative checks focusing on the realism of each and all simulated hydrologic variables (e.g., *ET*, Q_{bf}, soil temperature, etc.) were performed.

3.3. Relationship of $\mathcal{H}$ With Other Hydrologic Variables

$\mathcal{H}$ is evaluated using the relative soil water deficit X defined in (2). Since MOBIDIC uses a dual-compartmentalized soil, the complexity of the capillary and gravity reservoirs, $\mathcal{H}_c$ and $\mathcal{H}_g$, defined as,

$$\mathcal{H}_c = \mathcal{H}_c(X_c), \quad X_c = \forall_{e,c} / \forall_{e,max} \tag{13}$$

$$\mathcal{H}_g = \mathcal{H}_g(X_g), \quad X_g = \forall_{e,g} / \forall_{e,max} \tag{14}$$

are also investigated.

In order to gain insights into the partitioning of water in different storages, the dynamics of water in capillary storage and in gravity storage are considered relative to total available storage. The range of X is the interval [0,1]. But since $\forall_{e,max}=W_{c,max}+W_{g,max}$, the range of X_c and X_g are only subsets of this interval,

$$X_c \in [0, W_{c,max}/\forall_{e,max}] \tag{15}$$

$$X_g \in [0, W_{g,max}/\forall_{e,max}] \tag{16}$$

$$X=X_c+X_g, \qquad X \in [0,1] \tag{17}$$

3.3.1. Basin Attributes as Predictors of $\mathcal{H}$

The characteristic distributions of $\forall_e$ are hypothesized to be related to observable basin attributes. As tests, the relationships between temporal mean of $\mathcal{H}$, $\mathcal{H}_c$, and $\mathcal{H}g$, to the following basin attributes are investigated for the basins in Table 2:

1. *Catchment area A* (km^2): A basic spatial scale predictor that characterizes the dampening of hydrologic response in most cases.
2. *Median slope* s_{50} : The gradient along hillslopes, which influences both surface and subsurface runoff generation.
3. $\log_{10}(A/s_{50})$ (km): The basin-scale equivalent of the topographic wetness index (TWI) of *Beven and Kirby* [1979].
4. *Relief ratio* r_r : The range in elevation, $z_{max}-z_{min}$, normalized by the length of the mainstream L. As opposed to s_{50}, this indicates the gradient along channels.
5. *Drainage density* D_d (km^{-1}): The ratio of total stream length to A. High D_d implies high channelization of precipitation and shorter residence time. This also indicates the extent of riparian zones.
6. *Mean soil moisture capacity* $\overline{\forall_{e,max}}$ (m): The spatial mean of the product of the saturated soil moisture content θ_{sat} and the depth d (m) of the modeled soil layer. With the precipitation forcing minus evapotranspiration, this measure yields the characteristic time scale of the basin storage change.
7. *Aridity* $\overline{E_p}/\bar{P}$: The ratio between the annual mean potential evaporation (computed based on *Penman* [1948]) divided by the annual mean precipitation.
8. *Infiltration ratio* I_r : The mean precipitation intensity i_s/t_s (mm/h) (mean storm depth i_s (mm) divided by mean storm duration t_s (h)) during a storm event divided by the basin-averaged soil hydraulic conductivity $\overline{K_s}$. I_r characterizes the propensity of the basin to stormflow runoff.

3.3.2. $\mathcal{H}$ as Predictor of Hydrologic Response

The utility of $\mathcal{H}$, $\mathcal{H}_c$, and $\mathcal{H}g$ to explain the basin response is also investigated by relating them with the flux-based measures of hydrologic response listed below. The overbar symbol indicates temporal average.

1. *ET efficiency* $\overline{ET}/\overline{E_p}$: Ratio of basin-averaged ET to the potential rate E_p.
2. *Runoff ratio* $\bar{Q}/\bar{P}$: Fraction of precipitation that becomes runoff.
3. *Base flow index BFI* ($\overline{Q_{bf}}/\bar{Q}$): Fraction of streamflow contributed by base flow.

4. Results and Discussion

4.1. Basin-Scale Partitioning of Precipitation

Table 4 lists the diagnostic information on the calibrations. The Pearson correlation R ranges from 0.83 to 0.95, while the absolute bias B ranges from 0.05 to 0.12. The basin-scale partitioning of precipitation is shown in Figure 4. Taking the test basins all together, there is no clear pattern. However, by grouping the basins based on catchment area, a consistent pattern emerges. As shown, for basins with similar catchment area, the basin with higher median slope has higher runoff ratio and lower ET efficiency. The net groundwater recharge constitutes only a small fraction of the annual precipitation in all the test basins especially in the large basins where the spatial mean of percolation and channel leakage are balanced by capillary rise and channel seepage.

Table 4. Performance of Calibrated Models (R—Pearson Correlation; B—Absolute Bias)

ID	S0	S1	S2	S3	T0	T2	T3
R	0.92	0.95	0.83	0.84	0.88	0.94	0.91
B	0.06	0.05	0.09	0.06	0.03	0.10	0.12

4.2. Hydrologic Complexity

Figure 5 shows the maps as well as the marginal PDFs of the temporal mean of relative soil water deficit, $\bar{x}$,

$$\bar{x}=\overline{\forall_e}/\forall_{e,max} \tag{18}$$

of basin S0 which is the least complex with $\mathcal{H}(\bar{x})=0.09$, and of basin T2 which is the most complex with $\mathcal{H}(\bar{x})=0.62$ among the test basins. The overbar denotes temporal average. Basin S0 $\bar{x}$ is concentrated within the interval [0.4,0.6] and its PDF is closer to a Dirac delta than a uniform distribution, i.e., the PDF is highly divergent from a uniform distribution. In contrast, basin T2 $\bar{x}$ spans almost the entire interval [0,1] and its PDF is closer to a uniform distribution than a Dirac delta, i.e., the PDF is not highly divergent from a uniform distribution.

Figure 6 shows the hyetograph and time series of $\mathcal{H}$, $\mathcal{H}_c$, and $\mathcal{H}_g$ for basins S2 and T2 that have comparable areas but diverse climates. For all test basins, the simulated period is 3 years but only 1 year is shown for illustration. First for S2 (top plot), there is marked seasonality with most of the year being dry and the months of November–February receiving almost all of the annual precipitation. The soil moisture distribution mode lags precipitation by about a month. In dry conditions, most of the gravity reservoirs are completely empty so $\mathcal{H}_g$ is low and its value corresponds to the complexity of the time-invariant maximum capacity of the gravity reservoirs, $\mathcal{H}_g^*$,

$$\mathcal{H}_g^*=\mathcal{H}_g\left(\forall_{e,g,max}/\forall_{e,max}\right) \tag{19}$$

In contrast, there is higher spatial variability in x_c so $\mathcal{H}_c$ contributes more of the total complexity $\mathcal{H}$. It should be noted that $\mathcal{H}$ is not additive and the sum of $\mathcal{H}_c$ and $\mathcal{H}_g$ does not necessarily have to equal $\mathcal{H}$. In wet conditions, the trend is reversed. Since the capillary reservoirs are more filled, $x_c \approx 0$ across the basin so $\mathcal{H}_c \to 0$. The gravity reservoirs are variably saturated so $\mathcal{H}_g$ is high and it accounts for most of the total complexity. In intermediate wetness conditions, e.g., mid-March 2004, $\mathcal{H}_c$ and $\mathcal{H}_g$ both contribute significantly to $\mathcal{H}$. Meanwhile, the temperate basin T2 (bottom plot) receives more precipitation and the seasonality is mild. As a result, the general condition in the basin is often closer to wet than dry so $\mathcal{H}_g$ contributes most of the total complexity.

From the time series, the minimum, mean, and maximum values of $\mathcal{H}$, $\mathcal{H}_c$, and $\mathcal{H}_g$ for each basin, are computed. The characteristic mean values, and their relationships with some of the tested basin attributes, are plotted in Figures 7–10. As pointed in the analysis of basin-scale precipitation partitioning, it is difficult to see relationships if all basins are analyzed together. More clear relationships are found by comparing only basins with similar climate or size. For instance, Figure 7 shows how the complexity indices vary with aridity for basins of similar spatial scale. Overall, the total complexity $\mathcal{H}$ (and also $\mathcal{H}_g$) is higher in temperate basins. This is consistent with the understanding that soil moisture is lower and upper-bounded so its variability is higher at intermediate wetness conditions, see e.g., *Lawrence and Hornberger* [2007]. Independently, $\mathcal{H}_c$ of T2 and T3 are lower than those of S2 and S3 because the capillary reservoirs in the temperate basins are often saturated, i.e., they are less hydrologically active. Smaller basins have greater complexity than their larger counterparts for the same climate. Figure 7 is limited to size and climate distinguishing features only.

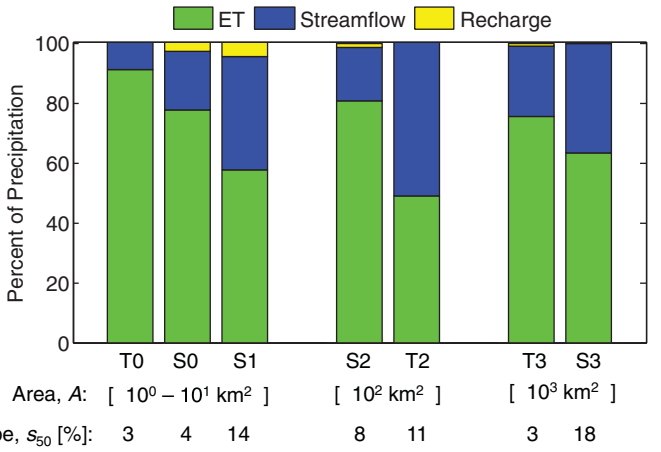

Figure 4. Basin-scale precipitation partitioning with basins grouped by catchment area and arranged in increasing median slope.

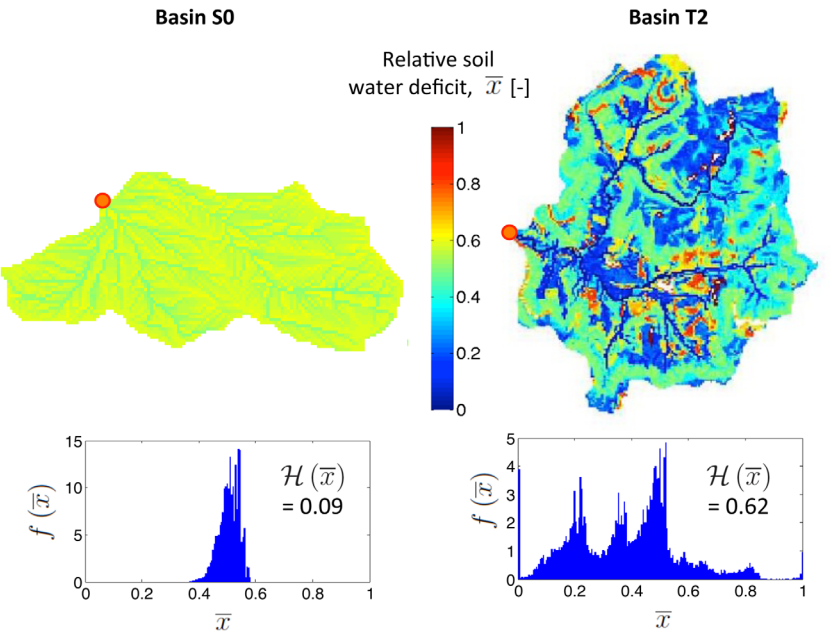

Figure 5. Map and PDF of characteristic (temporal mean) relative soil water deficit, $\bar{x} = \overline{\forall_e}/\forall_{e,max}$ of basins (left) S0 and (right) T2. Orange dots mark basin outlets.

Figure 8 shows that for both the semiarid and temperate test basins, $\mathcal{H}$, $\mathcal{H}_c$, and $\mathcal{H}_g$ generally increase with catchment area $\log_{10}A$ (top plots). The relationships with the basin-scale analog of topographic wetness index $\log_{10}(A/s_{50})$ (bottom plots) are practically the same as with $\log_{10}A$, with marginal improvement for the semiarid basins and marginal degradation for the temperate basins. Furthermore, Figures 9 and 10 show that $\mathcal{H}$, $\mathcal{H}_c$, and $\mathcal{H}_g$ are inversely related to relief ratio, and proportionally related to infiltration ratio. Weaker or no significant relationships are found for the other basin attributes considered.

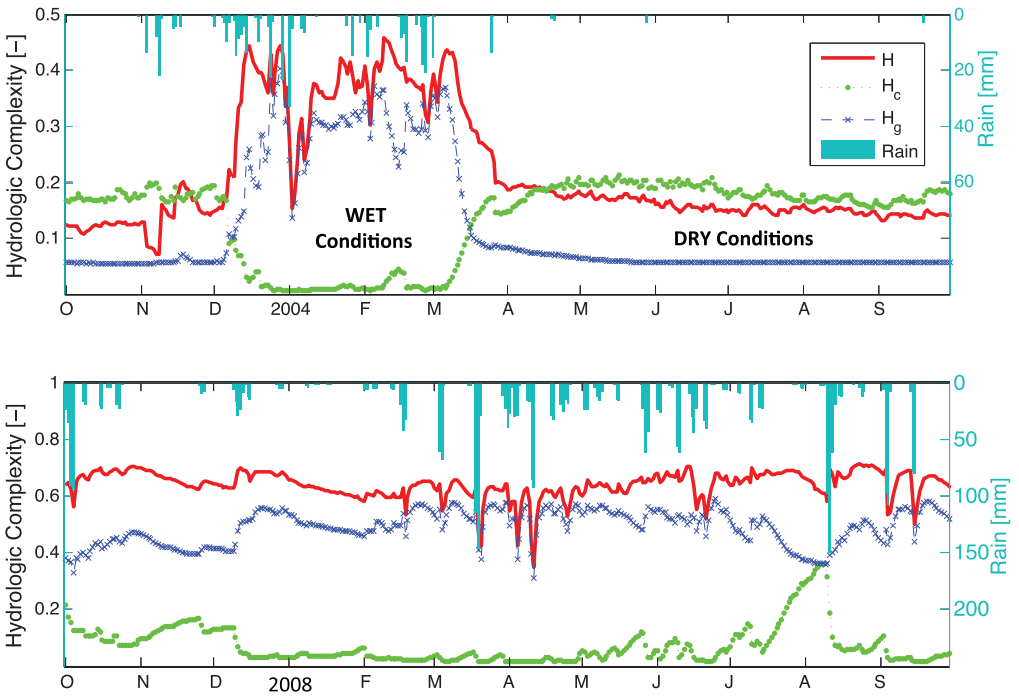

Figure 6. Time series of $\mathcal{H}$, $\mathcal{H}_c$, and $\mathcal{H}_g$ for basins (top) S2, and (bottom) T2.

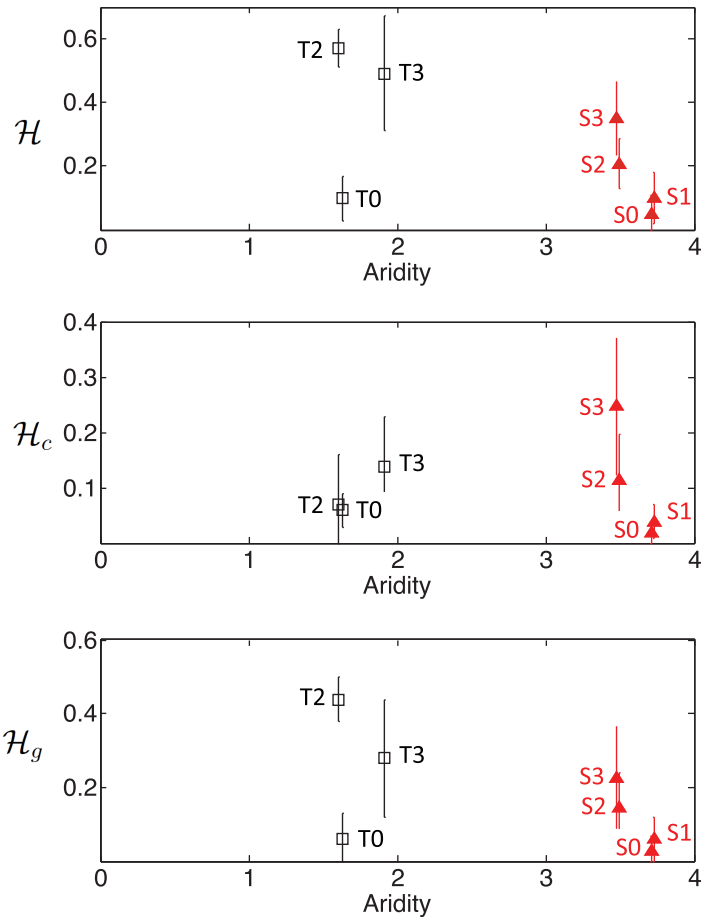

Figure 7. Temporal mean of (from top) $\mathcal{H}$, $\mathcal{H}_c$, and $\mathcal{H}_g$, versus aridity for semiarid and temperate test basins. Squares and triangles are temporal mean, respectively.

Figure 11 shows the relationship between the temporal mean of the complexity indices with three traditional measures of hydrologic response. The top row shows that the ET efficiency is practically independent of the complexity indices. In fact and as expected, ET efficiency is mainly a function of aridity. The middle row shows that the runoff ratio generally increases with $\mathcal{H}$, $\mathcal{H}_c$, or $\mathcal{H}_g$. Basins with higher value hydrologic complexity have a higher runoff ratio because storms with varied magnitudes (storm totals) contribute to runoff. In less complex basins, only storms of a certain magnitude and higher lead to runoff generation. This is evident in the stronger relationship between runoff ratio and $\mathcal{H}_g$ when compared to $\mathcal{H}_c$ (middle row of Figure 11). The base flow fraction of total basin streamflow (BFI) is proportional to the hydrologic complexity of the basins (bottom-left plot in Figure 11). The relationship is principally due to the $\mathcal{H}_g$ of the basins. With greater range in the distribution of soil moisture across the basin, the drainage of the basin during interstorm periods can persist for longer and become a more important component of basin outflow. The relationships with runoff ratio or BFI are stronger with $\mathcal{H}$ or $\mathcal{H}_g$, than with $\mathcal{H}_c$, because the state of the capillary reservoirs have less influence on runoff.

5. Summary and Conclusions

Basin response and hydrologic fluxes are functions of hydrologic states, most notably of soil moisture. To characterize the spatial distribution of soil moisture and understand its evolution in time, we introduced a modified version of the *Martina and Entekhabi* [2006] dimensionless index of hydrologic complexity $\mathcal{H}$ which measures the distance of a given distribution from two limiting distributions: Dirac delta and uniform distribution. The modifications make $\mathcal{H}$ invariant to discretization. The modified $\mathcal{H}$ is based on differential entropy, and is computed for a dimensionless random variable that is strictly in the interval [0,1]. Here the relative soil water deficit $\bar{x}$ is used. $\mathcal{H}$ is independent of the arrangement or clustering of the marginal probabilities of a given PDF, whereas the commonly used coefficient of variation is not since it depends on the mean of the PDF.

For demonstration, $\mathcal{H}$ is applied on seven test basins with area ranging from 10^0 to 10^3 km^2 and representing semiarid and temperate climates. Calibrated models of these basins are developed using the distributed hydrologic model MOBIDIC. While best efforts were done to ensure accuracy and realism of the calibrated models, it should be noted that the findings of this study are associated with model assumptions. Since a key feature of MOBIDIC is the partitioning of each pixel of soil into gravity reservoir and capillary reservoirs, we also investigated the complexity of these subsystems, $\mathcal{H}_c$ and $\mathcal{H}_g$, respectively. We show that $\mathcal{H}$, $\mathcal{H}_c$,

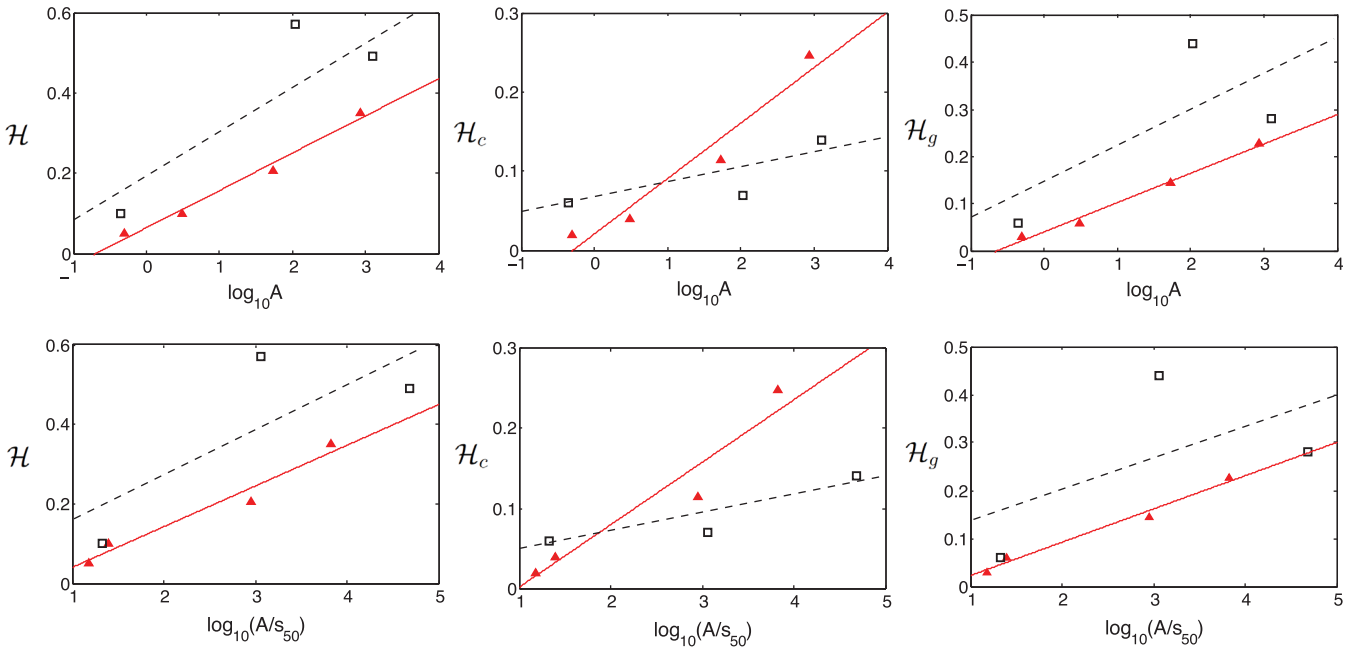

Figure 8. Temporal mean of (left to right) $\mathcal{H}$, $\mathcal{H}_c$, and $\mathcal{H}_g$, versus spatial scales: (top) catchment area $\log_{10}A$ (km^2), and (bottom) basin-scale topographic wetness index $\log_{10}(A/s_{50})$. Trend lines: solid for semiarid basins; and dashed for temperate basins.

and $\mathcal{H}_g$, track the evolution of the distributional features of soil moisture. In dry conditions, the gravity reservoirs are mostly empty so $\mathcal{H}_g$ is low and its value corresponds to the complexity of the time-invariant maximum capacity of the gravity reservoirs, $\mathcal{H}_g^*$. In contrast, there is higher spatial variability in the content of the capillary reservoirs so $\mathcal{H}_c$ is higher and contributes more to the total complexity $\mathcal{H}$. In wet conditions, the capillary reservoirs are mostly saturated so $\mathcal{H}_c \to 0$ while the gravity reservoirs are variably saturated so $\mathcal{H}_g$ is high and it contributes most of $\mathcal{H}$.

This paper also explored what and how basin attributes affect the characteristic value of $\mathcal{H}$, $\mathcal{H}_c$, and $\mathcal{H}_g$, and how these complexity indices can be used to explain interbasin variability in hydrologic response. Clear and meaningful relationships are found only when basins with the same climate or size are grouped. For basins of similar size, $\mathcal{H}$ and $\mathcal{H}_g$ are highest in temperate climate, consistent with soil moisture being lower-bounded so its variability is higher at intermediate values. $\mathcal{H}_c$ generally increases with aridity since the capillary reservoirs are often saturated in the temperate basins, i.e., they are less hydrologically active, and processes controlled by the state of the capillary reservoirs, e.g., ET, are more important in arid environments. Grouping basins with the same climate, it was found that (i) $\mathcal{H}$, $\mathcal{H}_c$, and $\mathcal{H}_g$, are proportionally related to catchment area, basin-scale topographic wetness index, and infiltration ratio, but inversely related to relief ratio. $\mathcal{H}$ and $\mathcal{H}_g$ are positively correlated with base flow index. No significant relationships are found for the

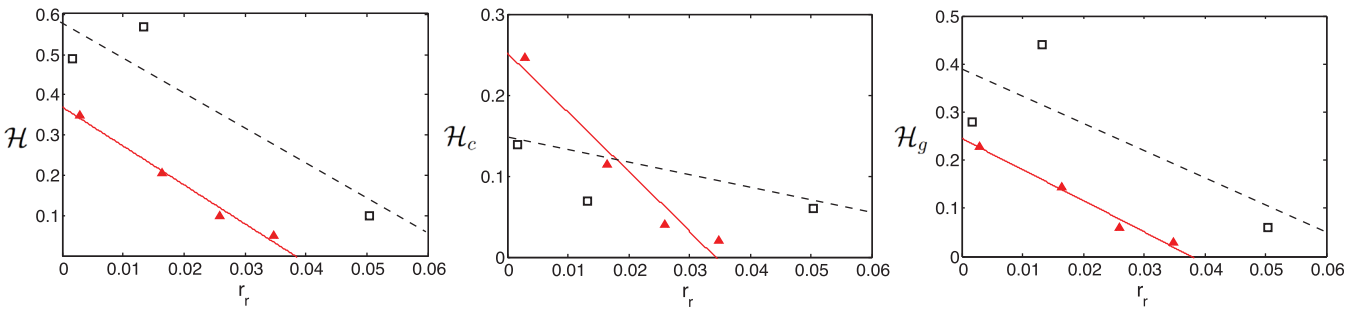

Figure 9. Temporal mean of (left to right) $\mathcal{H}$, $\mathcal{H}_c$, and $\mathcal{H}_g$, versus relief ratio r_r. Trend lines: solid for semiarid basins; and dashed for temperate basins.

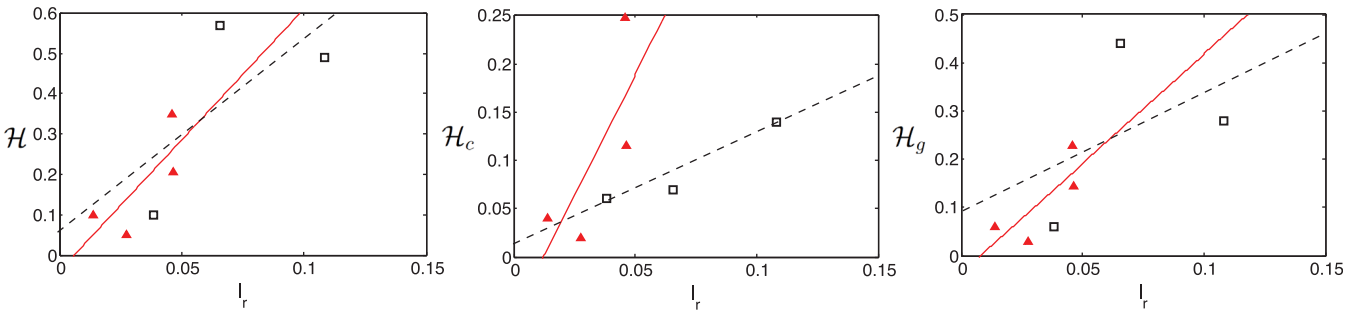

Figure 10. Temporal mean of (left to right) $\mathcal{H}$, $\mathcal{H}_c$, and $\mathcal{H}_g$, versus infiltration ratio I_r . Trend lines: solid for semiarid basins; and dashed for temperate basins.

other basin attributes considered, as well as with ET efficiency and runoff ratio. The current study is exploratory and tests with more basins with various settings, scales, and climates, are needed to verify the relationships found.

Limitations of the current approach include: (1) the lack of testing with directly observed soil moisture fields at fine spatial and temporal resolution, (2) accounting for different types of runoff generation such as

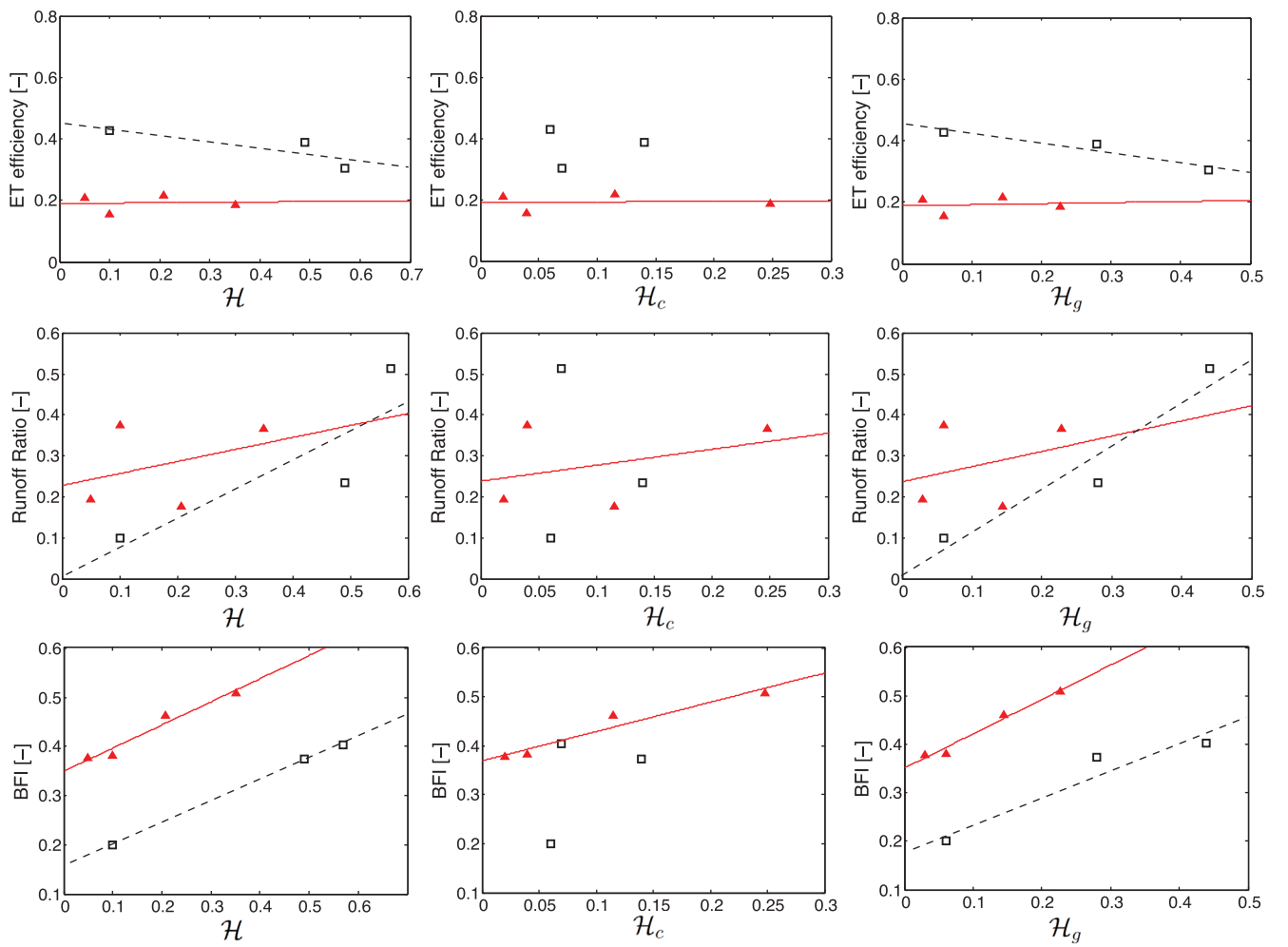

Figure 11. Temporal mean of (left to right) $\mathcal{H}$, $\mathcal{H}_c$, and $\mathcal{H}_g$, versus (top to bottom) ET efficiency, runoff ratio, and BFI. Trend lines: solid for semiarid basins; and dashed for temperate basins.

infiltration excess, (3) treatment of seasonal snow, snowpack, and snowmelt, and (4) incorporation of case-specific hydrogeological factors such as fractured bedrock and surface features such as rock outcrops, among others. The focus is on hydrologic response factors that can be considered shared and common among many but not all catchment, i.e., surface soil reservoir fill and runoff generation during storm and redistribution events. Some future research directions should address these limitations. Some, such as lack of space-time direct observations of soil moisture fields may be binding constraints today but feasible in the future. Snow processes and different mechanisms of runoff generation may be added. Hydrogeological and other case-specific complexities cannot be generalized and have to be dealt with in each case distinctly.

Acknowledgments
This research is funded in part by the Singapore National Research Foundation (NRF) through the Singapore-MIT Alliance for Research and Technology (SMART) Center for Environmental Sensing and Monitoring (CENSAM). Essential data sets used in this study are included as supplementary data. Additional data will be provided upon request.

References

Berger, K. P., and D. Entekhabi (2001), Basin hydrologic response relations to distributed physiographic descriptors and climate, *J. Hydrol.*, *247*, 169–182, doi:10.1016/S0022-1694(01)00383-3.

Beven, K. J., and M. J. Kirby (1979), A physically based, variable contributing area model of basin hydrology, *Hydrol. Sci. Bull.*, *24*(1), 43–69, doi:10.1080/02626667909491834.

Beven, K. J., and M. J. Kirby (1997), TOPMODEL: A critique, *Hydrol. Processes*, *11*, 1069–1085.

Buttle, J. M., P. J. Dillon, and G. R. Eerkes (2004), Hydrologic coupling of slopes, riparian zones and streams: An example form the Canadian Shield, *J. Hydrol.*, *287*, 161–177, doi:10.1016/j.jhydrol.2003.09.022.

Castelli, F., G. Menduni, and B. Mazzanti (2006), Use of multi-platform, multi-temporal remote-sensing data for calibration of a distributed hydrologic model: An application in the Arno basin, Italy, *Hydrol. Processes*, *20*, 2693–2712, doi:10.1002/hyp.6061.

Castelli, F., G. Menduni, and B. Mazzanti (2009), A distributed package for sustainable water management: A case study in the Arno basin, *IAHS Publ.*, *327*, 52–91.

Castillo, A. E. (2014), *Spatiotemporal variability of hydrologic response: An entropy-based approach using a distributed hydrologic model, PhD thesis*, Mass. Inst. of Technol., Cambridge, U. K.

Castillo, A. E., F. Castelli, and D. Entekhabi (2014), Gravitational and capillary soil moisture dynamics for hillslope-resolving models, *Hydrol. Earth Syst. Sci. Discuss.*, *7133–7168*, doi:10.5194/hessd-11-7133-2014. [Available at http://library.mit.edu/item/002293980.]

Cerdan, O., Y. L. Bissonnais, G. Govers, V. Lecomte, K. van Oost, A. Couturier, C. King, and N. Dubreuli (2004), Scale effect on runoff from experimental plots to catchments in agricultural areas in Normandy, *J. Hydrol.*, *1–2*, 4–14, doi:10.1016/j.jhydrol.2004.02.017.

Di Lazzaro, M. (2008), Correlation between channel and hillslope lengths and its effects on the hydrologic response, *J. Hydrol.*, *362*, 260–273, doi:10.1016/j.jhydrol.2008.08.022.

Diek, S., A. J. A. M. Temme, and A. J. Teuling (2014), The effect of spatial soil variation on the hydrology of a semi-arid rocky mountains catchment, *Geoderma*, *235–236*, 113–126, doi:10.1016/j.geoderma.2014.06.028.

Dorigo, W. A., et al. (2011), The international soil moisture network: A data hosting facility for global in-situ soil measurements, *Hydrol. Earth Syst. Sci.*, *15*, 1675–1698.

Famiglietti, J. S., J. A. Devereaux, C. A. Laymon, T. Tsegaye, P. R. Houser, T. J. Jackson, S. T. Graham, M. Rodell and P. J. vanOevelen (1999), Ground-based investigation of soil moisture variability within remote sensing footprints during the Southern Great Plains 1997 (SGP97) Hydrology Experiment, *Water Resour. Res.*, *35*(6), 1839–1851, doi:10.1029/1999WR900047.

Famiglietti, J., D. Ryu, A. A. Berg, M. Rodell, and T. J. Jackson (2008), Field observations of soil moisture variability across scales, *Water Resour. Res.*, *44*, W01423, doi:10.1029/2006WR005804.

Fernandez, J. M., and A. Ceballos (2003), Temporal stability of soil moisture in a large-field experiment in Spain, *Soil Sci. Soc. Am. J.*, *67*, 1647–1656, doi:10.2136/sssaj2003.1647.

Grayson, R. B., A. W. Wetern, F. H. Chiew, and G. Blöschl (1997), Preferred states in spatial soil moisture patterns: Local and nonlocal controls, *Water Resour. Res.*, *33*(12), 2897–2908.

Lawrence, J. E., and G. M. Hornberger (2007), Soil moisture variability across climate zones, *Geophys. Res. Lett.*, *34*, L20402, doi:10.1029/2007GL031382.

Mahmood, T. H., and E. R. Vivoni (2008), Evaluation of distributed soil moisture simulations through field observations during the North American Monsoon in Redondo Creek, New Mexico, *Ecohydrology*, *1*(3), 271–287, doi:10.1002/eco.23.

Mahmood, T. H., and E. R. Vivoni (2011), A climate-induced threshold in hydrologic response in a semiarid ponderosa pine hillslope, *Water Resour. Res.*, *47*, W09529, doi:10.1029/2011WR010384.

Martina, M. L., and D. Entekhabi (2006), Identification of runoff generation spatial distribution using conventional hydrologic gauge time series, *Water Resour. Res.*, *42*, W08431, doi:10.1029/2005WR004783.

Mendez-Barroso, L. A., and E. R. Vivoni (2010), Observed shifts in land surface conditions during the North American Monsoon: Implications for a vegetation-rainfall feedback mechanism, *J. Arid Environ.*, *74*(5), 549–555, doi:10.1016/j.jaridenv.2009.09.026.

Mendez-Barroso, L. A., E. R. Vivoni, A. Robles-Morua, G. Mascaro, E. Yepez, J. C. Rodriguez, C. J. Watts, J. Garatuza-Payan, and J. Saiz-Hernandez (2014), A modeling approach reveals differences in evapotranspiration and its partitioning in two semiarid ecosystems in Northwest Mexico, *Water Resour. Res.*, *50*, 3229–3252, doi:10.1002/2013WR014838.

Merz, R., G. Blöschl, and J. Parajka (2006), Spatio-temporal variability of event runoff coefficients, *J. Hydrol.*, *331*, 591–604, doi:10.1016/j.jhydrol.2006.06.008.

Meyles, E., A. Williams, L. Ternan, and J. Dowd (2003), Runoff generation in relation to soil moisture patterns in a small Dartmoor catchment, Southwest England, *Hydrol. Processes*, *17*, 251–264, doi:10.1002/hyp.1122.

Michalowicz, J. V., J. M. Nichols, and F. Bucholtz (2014), *Handbook of Differential Entropy*, CRC Press, Boca Raton, Fla.

Moghaddam, M., A. Silva, R. Akbar, D. Clewley, M. Burgin, A. Castillo, and D. Entekhabi (2013), *SoilSCAPE in situ network for multi-scale validation of SMAP data products, paper presented at International Geoscience and Remote Sensing Symposium (IGARSS)*, Institute of Electrical and Electronics Engineers, Melbourne, Australia.

Nippgen, F. B., L. McGlynn, L. A. Marshall, and R. E. Emanuel (2011), Landscape structure and climate influences on hydrologic response, *Water Resour. Res.*, *47*, W12528, doi:10.1029/2011WR011161.

Penman, H. L. (1948), Natural evaporation from open water, bare soil and grass, *Proc. R. Soc. London, Ser. A*, *193*, 120–145.

Penna, D., M. Borga, D. Norbiato, and G. Dalla (2009), Hillslope scale soil moisture variability in a steep alpine terrain, *J. Hydrol.*, *364*(3–4), 311–327, doi:10.1016/j.jhydrol.2008.11.009.

Rawls, W. J., D. L. Brakensiek, and K. E. Saxton (1982), Estimation of soil water properties, *Trans. Am. Soc. Civ. Eng.*, *25*(5), 1316–1321.

Reed, S., V. Koren, M. Smith, Z. Zhang, F. Moreda, D. J. Seo, and DMIP Participants (2004), Overall DMIP results, *J. Hydrol.*, *298*, 27–60, doi: 10.1016/j.jhydrol.2004.03.031.

Rodriguez-Iturbe, I., and A. Rinaldo (1997), *Fractal River Basins: Chance and Self-Organization*, Cambridge Univ. Press, N. Y.

Sankarasubramanian, A., and R. M. Vogel (2002), Comment on the paper: Basin hydrologic response relations to distributed physiographic descriptors and climate by Karen Plaut Berger, Dara Entekhabi, 2001. Journal of Hydrology, 247, 169–182, *J. Hydrol.*, *263*, 257–261.

Sefton, C. E., and S. M. Howarth (1998), Relationships between dynamic response characteristics and physical descriptors of catchments in England and Wales, *J. Hydrol.*, *211*, 1–6.

Singh, V. P. (2011), Hydrologic synthesis using entropy theory: Review, *J. Hydrol. Eng.*, *16(5)*, 421–433.

Tarbonton, D. G. (1997), A new method for the determination of flow directions and upslope areas in grid Digital Elevation Models, *Water Resour. Res.*, *33*(2), 309–319, doi:10.1029/96WR03137.

Teuling, A., and P. Troch (2005), Improved understanding of soil moisture variability dynamics, *Geophys. Res. Lett.*, *32*, L05404, doi:10.1029/2004GL021935.

van Dijk, A. I. J. M. (2010), Climate and terrain factors explaining streamflow response and recession in Australian catchments, *Hydrol. Earth Syst. Sci.*, *14*, 159–169. [Available at http://www.hydrol-earth-syst-sci.net/14/159/2010/hess-14-159-2010.pdf.]

Vivoni, E. R., D. Entekhabi, R. L. Bras, and V. Y. Ivanov (2007), Controls on runoff generation and scale-dependence in a distributed hydrologic model, *Hydrol. Earth Syst. Sci.*, *4*, 1–47.

Zecharias, Y. B., and W. Brutsaert (1988), The influence of basin morphology on groundwater outflow, *Water Resour. Res.*, *24*(10), 1645–1650.